Vertical error distribution of ASTER GDEM V2 data based on ICESat/GLA14 data: taking Shanxi Plateau of China as an example

Shangmin Zhao
Department of Surveying and Mapping, College of Mining Engineering
Taiyuan University of Technology
Taiyuan, China
zhaoshangmin@tyut.edu.cn

Li Wang
Department of Surveying and Mapping, College of Mining Engineering
Taiyuan University of Technology
Taiyuan, China
wl3001@link.tyut.edu.cn

Wenjiao Wu
Department of Surveying and Mapping, College of Mining Engineering
Taiyuan University of Technology
Taiyuan, China
wwj3256@link.tyut.edu.cn

Abstract—**Taking Shanxi Plateau of China as an example, this study aims to quantitatively analyze the vertical error distribution of the ASTER GDEM V2 data using ICESat/GLA14 data as the benchmark data. The ASTER GDEM V2 and ICESat/GLA14 data were downloaded from USGS and NSIDC respectively, and the ICESat/GLA14 data was used to derive distribution of vertical errors in ASTER GDEM V2 data in the study area firstly; then, the study area was divided into geomorphic units at third class levels, the whole Shanxi Plateau, three regions and eleven subregions. In addition, vertical error distributions were analyzed in these divided geomorphic units; finally, the vertical error distributions among the topographic, landuse and NDVI classes were analyzed. The results show that the vertical error distribution presents a normal distribution in the study area, whose mean and RMSE values are -0.1m and 11.8m respectively. The study area is divided into three geomorphic regions: Central Basin, western Lvliang Mountain and eastern Taihang Mountain; the mean values of the vertical error are 1.1m, 0.0m and -0.6m respectively in the three regions. As to the RMSE values, 9.1m, 12.2m and 12.6m respectively; so the vertical error is low in the middle basin region, but high in the mountain regions of the two sides.With the values of the topographic factors (elevation, slope and relief) increasing, the value of the vertical error becomes higher accordingly. As to the aspect factor, the vertical error is symmetrical along the NE-SW axis; besides, the NE and SW directions has highest positive and negative values respectively. To the NDVI factor, the vertical error decreases with the NDVI values increasing generally; to the land use factor, the highest vertical error distributes in the forestland and grassland.**

Keywords: **vertical error distribution; ASTER GDEM V2; ICESat/GLA14; geomorphic unit; Shanxi Plateau**

I. INTRODUCTION

Digital Elevation model (DEM) data can provide significant information for many research activities [1, 2]. As one of the most used global DEM dataset, ASTER GDEM (Advanced Spaceborne Thermal Emission and Reflection Radiometer Global Digital Elevation Model) V2 data has high spatial resolution (1″) and wide coverage (83ºN–83ºS). So it is used in many applications after its release. Because the feasibility of the application using DEM data depends on its accuracy [3], it is meaningful for estimating the accuracy of the ASTER GDEM V2 data [4]. In this study, we use the ICEsat/GLA14 (the 14the product of the Geoscience Laser Altimeter System on the Ice, Cloud, and land Elevation Satellite) data to provide to an unbiased estimate of the regional accuracy of ASTER GDEM V2 data in the Shanxi Plateau of China, because the ICESat/GLA14 data has high (0.1 m (1σ) for flat bald locations and 1 m (1σ) for undulated and vegetated surface) [5].

II. STUDY AREA

The location of the study area is shown in Fig.1. From Fig.1, the study area is the Shanxi Plateau, which locates in the northern and eastern of China. With Yellow River adjoining the western and southern side, many rivers in the Shanxi Plateau flow into the Yellow River. Shanxi Plateau distributes in the eastern part of the Loess Plateau, so there is deep loess covering here.

The study area presents nearly north-south direction. With Lvliang Moutain and Taihang Mountain in its western and eastern side, there are many intermountain basins in its middle part, such as Datong Basin and Taiyuan Basin.

According to the topographic characterisitcs, the study area is divided into three geomorphic regions. These can be further divided into 12 subregions, which are shown in Fig.1.

In: Geomorphometry for Geosciences, Jasiewicz J., Zwoliński Zb., Mitasova H., Hengl T. (eds), 2015. Adam Mickiewicz University in Poznań - Institute of Geoecology and Geoinformation, International Society for Geomorphometry, Poznań

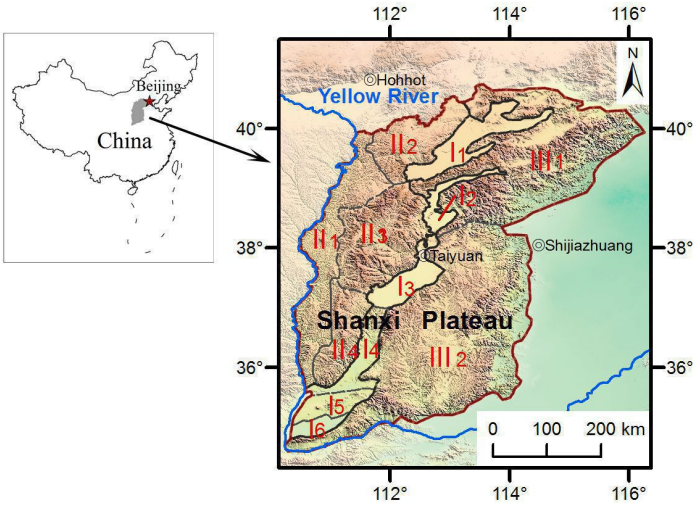

Figure 1. Location and geomorphic units in the study area

In Figure 1, I: Central Basin Region; I_1: Datong Basin Subregion; I_2: Xinding Basin Subregion; I_3: Taiyuan Basin Subregion; I_4: Linfen Basin Subregion; I_5: Emei Platform Subregion; I_6: Yuncheng Basin Subregion; II: Lvliang Mountain Region; II_1: Western Lvliang Mountain Subegion; II_2: Northern Lvliang Mountain Subegion; II_3: Central Lvliang Mountain Subegion; II_4: Southern Lvliang Mountain Subegion; III: Taihang Mountain Region; III_1: Northern Taihang Mountain Subregion; III_2: Southern Taihang Mountain Subregion.

III. METHODOLOGY AND RESULTS

A. Data Process

The data used in this research are mainly ASTER GDEM V2 data and ICESat/GLA14 data.

ASTER GDEM V2 data is the version 2 of the ASTER GDEM, which is an upgrade to version 1 and developed using an advanced algorithm and more data sources. Downloaded from USGS Global Data Explorer, the ASTER GDEM V2 data is processed through mosaic, projection and clipping, which is shown in Fig.2.

ICESat/GLA14 is collected through collected through the U.S. National Snow & Ice Data Centre (NSIDC), and extracted by NGAT tools. The extracted results have 19 phases from 2003 to 2009. The original value is reference to the Topex/Poseidon ellipsoid, so it needs to be transformed to reference the WGS84 ellipsoid using the following equation:

$$ICESat_{\_WGS84} = ICESat_{\_TOPEX} - ICESat_{\_geoid} - Offset \quad (1)$$

where $ICESat_{\_TOPEX}$ and $ICESat_{\_geoid}$ can be directly acquired from the ICESat/GLA14 data, the Offset is a constant, 0.7m[6].

Then, overlapping all the ICESat/GLA14 data 19 phases and clipped by the boundary, the result is shown in Fig.3.

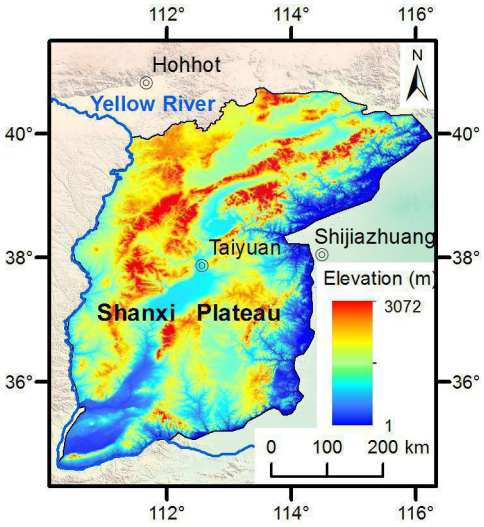

Figure 2. ASTER GDEM V2 data in the study area

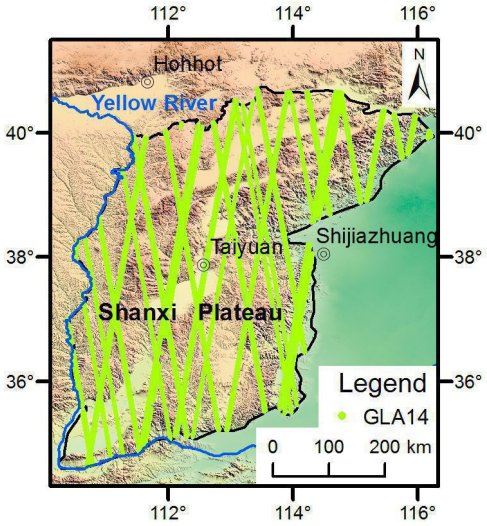

Figure 3. ICESat/GLA14 data in the study area

B. Vertical Error Distribution in the Study Area

Taking the ICESat/GLA14 data as the real value, the difference between the ICESat/GLA14 and ASTER GDEM V2 data is regareded as the vertical error. After removing the ICESat/GLA14 outliers and taking 1m as the interval, the histrogram of the vertical error in the study area is shown in Fig.4, which shows that the vertical error presents a normal distribution.

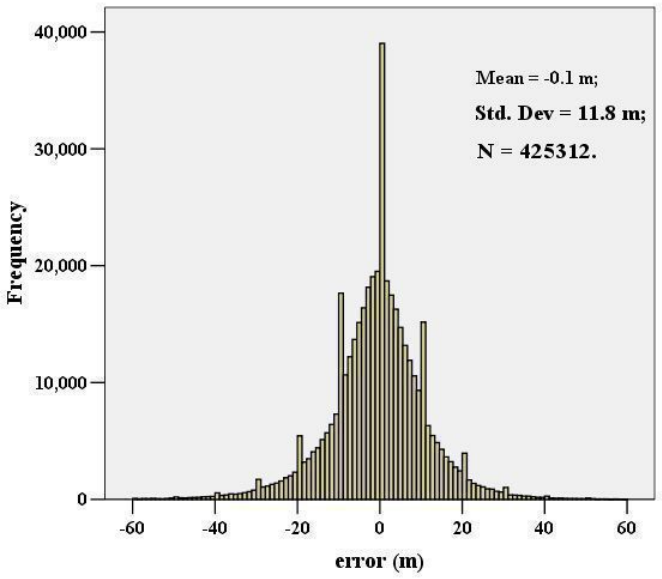

Figure 4. Vertical error distribution frequency in the study area

C. *Vertical Error Distribution in the Geomorphic Units*

The study area is divided into three geomorphic regions, the name and distribution of which are shown in Fig.1. The vertical error stattistics in the three geomorphic regions are computed in Tab.1, which shows thta the vertical error is low in th middle basin, but high in the sides mountains, and the western Lvliang Mountains has highest error values.

TABLE I. VERTICAL ERROR DISTRIBUTION IN GEOMORPHIC REGION (M)

geomorphic unit	vertical error statistics			
	samples	*mean*	*standard deviation*	*RMSE*
I	70666	1.1	9.0	9.1
II	117336	0.0	12.6	12.6
III	237310	-0.6	12.2	12.2

The Three geomorphic regions are re-divided into 12 geomorphic subregions, the vertical error stasitics of which can be shown in Tab.2, which shows: except for the northern Datong Bazsin, from north to south, the vertical error becomes high for the middle basins; this is also suitable for the western Lvliang Mountains, except for the Western Lvliang Moutain subregion; as to the eastern Taihang Mountain, the error is high in the north part but low in the south part, the reason may be because the northern part is steeper than the sourthern part.

TABLE II. VERTICAL ERROR DISTRIBUTION IN GEOMORPHIC SUBREGION (M)

unit	vertical error statistics			unit	vertical error statistics		
	mean	*Std.* [a]	*RMSE*		*mean*	*Std.* [a]	*RMSE*
I_1	-0.4	8.5	8.5	II_1	0.5	12.6	12.6
I_2	-0.7	7.3	7.3	II_2	-1.0	9.2	9.2
I_3	0.9	7.2	7.3	II_3	-0.6	12.2	12.2
I_4	0.7	8.9	9.0	II_4	1.2	15.3	15.4
I_5	4.2	11.4	12.1	III_1	-1.9	12.3	12.5
I_6	7.1	10.4	12.6	III_2	0.3	12.0	12.0

a. Standard deviation value. This is the same for the following cases.

D. *Vertical Error Distribution among the Topographic Factors*

Using the ArcGIS software, the topographic factors are computed using ASTER GDEM V2 data, which are elevation, relief, slope and aspect. Then this factors are classfied by the values. The vertical error statistics in the classes for the elevation factor are shown in Tab.3 (As the standared deviaiton value is simlar to the RMSE value, the RMSE values are ommited in the following tables to reduce space).

Tab.3 shows: with the elevation value increasing, the error changes from positive value to negative values. The absolute error and standard deviation values presents increasing tendency.

TABLE III. VERTICAL ERROR DISTRIBUTION FOR ELEVATION FACTOR (M)

class	*mean*	*Std.*	class	*mean*	*Std.*
<=500	3.2	10.5	2000-2500	-5.7	12.7
500-1000	0.1	12.7	2500-3000	-7.3	13.6
1000-1500	-1.4	13.3	>3000	-10.1	17.3
1500-2000	-2.6	12.9			

The relief factor is computed using 20*20 windows, and the vertical error distribution for the relief factor is acquired in Tab.4, which shows that the absolute error and standard deviation values increase continuously.

TABLE IV. VERTICAL ERROR DISTRIBUTION FOR RELIEF FACTOR (M)

class	*mean*	*Std.*	class	*mean*	*Std.*
<=50	1.1	7.3	200-500	-5.3	17.5
50-200	-1.2	13.0	>500	-12.0	24.1

The error distribution for the slope factor is acquired in Tab. 5, which shows: with the slope value increases, the mean value of the vertical error changes from positive value to negative value,

and decreases continuously; meanwhile, the standard deviation value increases continuously.

TABLE V. VERTICAL ERROR DISTRIBUTION FOR SLOPE FACTOR (M)

class(°)	*mean*	*Std.*	class(°)	*mean*	*Std.*
<=3	0.5	6.8	15-25	-1.9	14.3
3-8	0.1	9.3	>25	-3.9	17.8
8-15	-0.9	12.2			

The vertical error distribution for the aspect factor is acquired in Tab. 6, which shows: the standard deviation values are similar in all the direction; as to the mean value, it is symmetrical along the NE-SW axis; besides, the NE and SW directions have highest positive and negative values respectively.

TABLE VI. VERTICAL ERROR DISTRIBUTION FOR ASPECT FACTOR (M)

class(°)	*mean*	*Std.*	class(°)	*mean*	*Std.*
Flat(-1)	1.6	11.4	S(167.5-202.5)	-4.2	12.3
N(337.5-22.5) [b]	3.2	12.4	SW(202.5-247.5)	-5.9	12.7
NE(22.5-67.5)	3.7	12.8	W(247.5-292.5)	-3.9	12.0
E(67.5-112.5)	2.5	13.1	NW(292.5-337.5)	-1.3	12.1
SE(112.5-167.5)	-0.8	12.5			

b. For "N", "337.5-22.5" means "337.5-360" or "0-22.5".

E. Vertical Error Distribution among the Land Cover Factors

In order to acquire the relationship among the vertical error distribution and the land cover factors, the NDVI and land use data were acquired from remote sensing images. The NDVI data is acquire in August, 2005, the mid acquisition time for both ASTER GDEM V2 and ICESat/GLA14 data. Through classification, the vertical error distribution for the NDVI is computed in Tab. 7, which shows: the standard deviation values are similar, but the mean value changes from negative to positive with the NDVI value increasing; when the NDVI value is higher than 0.8, the mean value return to negative value.

TABLE VII. VERTICAL ERROR DISTRIBUTION FOR NDVI FACTOR (M)

class	*mean*	*Std.*	class	*mean*	*Std.*
< 0.2	-4.2	12.3	0.6-0.8	0.3	12.1
0.2-0.4	-2.0	12.6	> 0.8	-1.2	14.5
0.4-0.6	-1.1	12.4			

The vertical error distribution for the land use factor can be shown in Tab.8, which shows: the highest error values distribute in the forestland and grassland, both for the mean and standard deviation values; as to other classes, the error values are similar.

TABLE VIII. VERTICAL ERROR DISTRIBUTION FOR LAND USE FACTOR (M)

class	*mean*	*Std.*	class	*mean*	*Std.*
paddy field	-0.3	11.1	water	-0.1	11.7
dry field	0.2	10.7	building	0.2	7.8
forestland	-2.2	15.3	unused	-1.4	9.3
grassland	-2.4	13.9			

IV. DISCUSSIONS

In order to make the research results more reasonable, the accuracy of the ICESat/GLA14 data should be estimated in the study area.

V. CONCLUSIONS

By using highly precise ICESat/GLA14 data, we have been able to analyze mean vertical accuracy of the ASTER GDEM v2 product over the study area. The research results show that the vertical errors are greatest for steep slopes, high relief and altitudes, forest and grassland and high NDVI. Bias is negative for high slope gradients, relief and altitude, and for west- and south-facing slopes.

ACKNOWLEDGMENT

This research is under the auspices of the National Natural Science Foundation of China (41301469, 41171332), the Open Foundation of the LREIS and the Qualified Personnel Foundation of Taiyuan University of Technology (QPFT) (tyut-rc201221a).

REFERENCES

[1] Guha, A., Singh, V. and Parveen, R., et al. 2013. "Analysis of ASTER data for mapping bauxite rich pockets within high altitude lateritic bauxite, Jharkhand, India". International Journal of Applied Earth Observation and Geoinformation, 21, 184-194.

[2] Frey, H. and Paul, F., 2012. "On the suitability of the SRTM DEM and ASTER GDEM for the compilation of topographic parameters in glacier inventories". International Journal of Applied Earth Observation and Geoinformation, 18, 480-490.

[3] Dragut, L. and Eisank, C., 2011. "Object representations at multiple scales from digital elevation models". Geomorphology 129: 183–189.

[4] Hengl, T. and Reuter, H., 2011. How accurate and usable is GDEM? A statistical assessment of GDEM using LiDAR data. In: GEOMORPHOMETRY, 45-48, Redlands.

[5] González, J., Bachmann, M. and Scheiber, R., et al. 2010. "Definition of ICESat Selection Criteria for Their Use as Height References for TanDEM-X". IEEE Transactions on Geoscience and Remote Sensing, 48, 2750-2757.

[6] Wang, X., Cheng, X. and Huang, H., et al. 2013. "DEM production for Dome-A combining GPS and GLAS data". Journal of Remote Sensing, 17(2), 439-444.